Journal of Engineering Technology and Applied Physics

Modeling of Capacitance in A Supercapacitor

Ah Heng You* and Pei Ling Cheang
Faculty of Engineering and Technology, Multimedia University, Jalan Ayer Keroh Lama, 75450, Melaka, Malaysia.
*ahyou@mmu.edu.my
https://doi.org/10.33093/jetap.2019.1.1.5

***Abstract* - A general supercapacitor model is developed by incorporating the effective surface area in the presence of pores. An analytical solution has been derived from the generic equation in Laplace domain based on the porous-electrode theory. This model demonstrates the effects of solution to matrix conductivity ratio, separator to electrode resistance ratio and discharge current density on the electrochemical impedance, capacitance and energy density of supercapacitor. The electrochemical impedance, capacitance and energy density of supercapacitor are calculated in this work. The maximum capacitance of 12.71 F/cm^2 was computed in low frequency range in this device. The proposed model can be applied to simulate the characteristics of polymer-based supercapacitor in near future.**

Keywords*—Supercapacitor, capacitance, electrochemical impedance, energy, modeling

I. Introduction

Supercapacitor is widely used in electric vehicles as a high power device. There are two mechanisms for energy storage in electrochemical capacitors i.e. double-layer charging process because of charge separation and a faradaic process because of redox reactions. It is also classified into two types namely double-layer (DL) capacitors and pseudocapacitors. Double-layer capacitor was extensively studied by determining the capacitance due to charge separation between an electrolyte and a metallic electrode [1, 2]. In the design of electrode, carbon materials are commonly used in double-layer capacitor because of the large interface area between the electrolyte and electrode. The activated carbon is another large surface area material normally used to achieve high energy density in double-layer capacitor. Posey *et al.* [3] derived macroscopic equations to describe the behavior of double-layer capacitors under potentiostatic and galvanostatic charging in porous electrodes. A DL model was proposed by Newman *et al.* [4, 5] to describe DL charging in an electrochemical cell. This model is able to estimate the specific energy and power densities of electrochemical capacitors.

Pseudocapacitors are introduced with relatively large surface area transition metal oxides such as amorphous $RuO_2.xH_2O$, CoO_x and NiO_x to improve the capacitor performance [6]. Pseudocapacitance is generated from the chemisorption of active ion or the faradaic redox reaction happening on the transition metal oxide. Ruthenium oxide, RuO_2 with carbon electrode is mostly applied in pseudocapacitor based on faradaic reactions. The faradaic process significantly enhances the energy density in the capacitor. Low power density and high cost make pure $RuO_2.xH_2O$ not suitable for electrochemical capacitor applications. Hence, nanostructured $RuO_2.xH_2O$-carbon composite materials with large surface area of porous activated carbon for high DL capacitance receive great interest recently.

The constant current operation of the capacitor using Tafel kinetics was reported by Shi [7]. It was suggested that the pores of different sizes (i.e. micro-, meso and macropores) play different roles in contributing to DL capacitance. Much of the charge storage occurs in pores with diameters less than 2 nm. The constant-current model was developed by Farahmandi [8] to investigate the effect of the ionic and electronic resistances of an electrochemical capacitor during the charging. A mathematical model using porous-electrode theory for an electrochemical capacitor was developed by Srinivasan *et al.* [9]. The analytical solutions were used to evaluate the capacitor performance under constant-current discharge and electrochemical impedance spectroscopy. DL capacitor model consists of two identical porous electrodes with a separator between them in the presence of electrolyte. The constant-current discharge model was applied to express the relationships of energy and power density of capacitor in terms of the physical parameters such as porosity, thickness etc.

A one-dimensional model using the theory of porous electrode for an electrochemical capacitor with hydrous ruthenium oxide ($RuO_2.xH_2O$) electrodes was studied by Lin *et al.* [10]. The double-layer and surface faradaic processes were considered in their model to predict the performance of the capacitor under conditions of galvanostatic charge and discharge. The effects of particle size and capacitor current density on the charge or discharge condition were studied. They showed that the energy density and discharge time could

Journal of Engineering Technology and Applied Physics (2019) 1, 1, 5: 18 - 23
https://doi.org/10.33093/jetap

Published by MMU PRESS. URL: https://journals.mmupress.com/index.php/jetap/index

be increased by decreasing the particle size in DL capacitor. DL process had the shortest discharge time than faradaic process. The particle-packing effects were included in a mathematical model of electrochemical capacitor consisting RuO_2 in porous activated carbon proposed by Lin *et al.* [11]. The effects of varying carbon type, carbon mass/volume fraction and discharge current density on the performance of RuO_2/C electrochemical capacitors was investigated using this model. The optimization of carbon content at moderate rate increased the charge delivery and energy density and minimized the cost of capacitor.

A pseudo two-dimensional model was developed by Kim *et al.* [12] to study RuO_2/carbon supercapacitors by including the diffusion of protons in the oxide particle using the superposition technique. The governing equations and concentrated solution theory were applied in this model to study the effect of particle size of oxide, porosity and the ratio of concentration of electrolyte in the electrode on pseudocapacitor and DL capacitor. They found that the small nanosize particles and high porosity electrode generated the highest energy density at 5 kW/kg thus reduce the cost of the supercapacitor.

The governing equations and the boundary conditions were generalized to model the capacitor using a current, potential or power excitation source by Verbrugge *et al.* [13]. A mathematical analysis based on porous electrode theory and a dilute-solution theory for the liquid phase within the pores of the electrode was employed. The influence of porosity and tortuosity on the transport parameters were incorporated in the carrier transport phenomena. Two phenomenological equations of ions transport by migration and diffusion, and molar flux of species away from the electrode surface due to charging and discharging of the electric double layer were employed for the liquid phase.

This work improves previous models [9, 10] for DL capacitance and faradaic redox reactions by using porous-electrode theory for varying composition and particle size effects on electrochemical capacitor performance. The effects of varying solution to matrix conductivity ratio, δ, the separator to electrode resistance ratio, α and the discharge current density on the electrochemical impedance, capacitance and energy density of supercapacitor were studied in this work. The supercapacitor model was then applied to compute the capacitance from Newman *et al.* [5] and Lin *et al.* [10] works in DL supercapacitor using the porous carbon electrodes.

II. Supercapacitor Model

The proposed supercapacitor model consists of two identical porous electrodes with a separator sandwiched between them as shown in Fig. 1. The potential of porous matrix and the potential of the solution in pores are denoted as ϕ_1 and ϕ_2.

The current densities in the matrix and solution phases are developed using Ohm' law as below

$$i_1 = -\sigma \frac{\partial \phi_1}{\partial x} \tag{1}$$

$$i_2 = -\eta \frac{\partial \phi_2}{\partial x} \tag{2}$$

, where σ and η are the matrix phase conductivity and effective conductivity of the electrolyte in electrode.

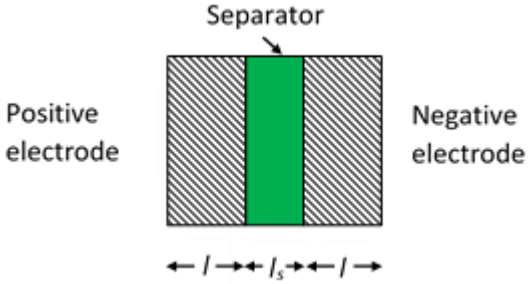

Fig. 1. The proposed supercapacitor model.

Based on the conservation of charge in the device, the total current is $I = i_1 + i_2$. The first derivatives of these current components are

$$\frac{\partial i_1}{\partial x} = -\frac{\partial i_2}{\partial x} = a i_T \tag{3}$$

, where a is the interfacial area per volume and i_T is the device current per interfacial area.

The relationship between the interfacial potential difference and the device current is expressed as

$$i_T = -C \frac{\partial(\phi_1 - \phi_2)}{\partial t} \tag{4}$$

, where C is the capacitance per interfacial area.

Hence, the normalized overpotential formula is

$$\frac{\partial^2 \varphi'}{\partial x'^2} = \frac{\partial \varphi'}{\partial \tau} \tag{5}$$

, where $\varphi' = \frac{\phi_1 - \phi_2}{V_o}$ is the normalized overpotential, $x' = \frac{x}{l}$ is the normalized distance and $\tau = \frac{\sigma \eta\, t}{acl^2(\sigma+\eta)}$ is the normalized discharge time.

By using Laplace transform, the solution for normalized overpotential in Eq. (5) is found to be

$$\bar{\varphi}'(x', s) = A\cosh\left(x'\sqrt{s}\right) + B\sinh\left(x'\sqrt{s}\right) \tag{6}$$

, where A and B are the constants at boundary conditions.

The solution phase current is derived as

$$i_2 = \left[\frac{\delta}{(1+\delta)} + \frac{1}{I'}\frac{\partial \varphi'}{\partial x'}\right] I \tag{7}$$

, where $\delta = \frac{\eta}{\sigma}$ is the ratio of solution to matrix phase conductivity and $I' = \frac{(\sigma+\eta)lI}{\sigma\eta V_o}$ is the normalized device current.

The device current consists of the matrix phase and solution phase currents at $x = 0$ and $x = l$. The boundary conditions are written as

$$x' = 0,\ \frac{\partial \varphi'}{\partial x'} = -\frac{\delta}{1+\delta} I' \quad (8)$$

$$x' = 1,\ \frac{\partial \varphi'}{\partial x'} = \frac{1}{1+\delta} I' \quad (9)$$

In the Laplace domain, the normalized overpotential is expressed in term of normalized device current after applying the boundary conditions from Eqs. (8) and (9) as

$$\bar{\varphi}' = \frac{\cosh(x'\sqrt{s}) + \delta\cosh((1-x')\sqrt{s})}{(1+\delta)\sqrt{s}\sinh(\sqrt{s})} \bar{I}' \quad (10)$$

Hence, the solution phase current yields

$$\bar{\imath}_2 = \left[\frac{\delta}{(1+\delta)} + \frac{\sinh(x'\sqrt{s}) - \delta\sinh((1-x')\sqrt{s})}{(1+\delta)\sinh(\sqrt{s})}\right]\bar{I} \quad (11)$$

The potential difference across the porous electrode is calculated as

$$\bar{\phi}_2|_{x'=0} - \bar{\phi}_2|_{x'=1} = \left[\frac{\delta}{(1+\delta)^2} + \frac{(\delta-1)(1-\cosh(\sqrt{s}))}{(1+\delta)^2\sqrt{s}\sinh(\sqrt{s})}\right]\bar{I}'V_o \quad (12)$$

The device voltage of two porous electrodes with a separator is written as

$$V_{Cell} = 2V_o - 2[(\phi_2|_{x'=0} - \phi_2|_{x'=1}) + \varphi|_{x'=0}V_o] - \frac{l_s I}{\eta_s} \quad (13)$$

, where l_s and η_s are the thickness and conductivity of separator.

The normalized device voltage in Laplace domain is obtained from the potential difference in Eq. (12) as

$$\bar{V}' = 1 - \frac{2\delta\bar{I}'}{(1+\delta)^2\sqrt{s}\sinh(\sqrt{s})} - \frac{(1+\delta^2)\coth(\sqrt{s})\bar{I}'}{(1+\delta)^2\sqrt{s}} - \frac{\delta\bar{I}'}{(1+\delta)^2} - \frac{\alpha\bar{I}'}{2} \quad (14)$$

, where $\alpha = \frac{\sigma\eta\, l_s}{(\sigma+\eta)\eta_s l}$ is the ratio of separator to electrode resistance.

Hence, normalized device voltage in time domain with constant current is expressed as

$$V' = \delta\phi - \frac{(1+3\delta+\delta^2)I'}{(1+\delta)^2} - \frac{2I'}{(1+\delta)^2}\sum_{n=1}^{\infty}[(-1)^n + \delta]^2 e^{-n^2\pi^2\tau} - \frac{\alpha I'}{2} \quad (15)$$

, where $\delta\phi$ is the delta function.

The normalized overpotential is expressed in time domain at each electrode in following:

$$\varphi' = I' + \frac{2I'}{(1+\delta)}\sum_{n=1}^{\infty}[(-1)^n + \delta]\cos(n\pi x')\, e^{-n^2\pi^2\tau} \quad (16)$$

The discharging current in supercapacitor is obtained by differentiating the normalized overpotential with respect to time. The device current per interfacial area is derived as

$$i_T = \frac{2I}{(1+\delta)al}\sum_{n=1}^{\infty}[(-1)^n + \delta]n^2\pi^2\cos(n\pi x')\, e^{-n^2\pi^2\tau}. \quad (17)$$

The impedance of the device is obtained by differentiating the normalized voltage with respect to the current. By replacing s with $j\omega'$ for a small sinusoidal perturbation voltage, the normalized impedance is

$$Z' = \frac{4\delta}{(1+\delta)^2\sqrt{j\omega'}\sinh(\sqrt{j\omega'})} + \frac{2(1+\delta^2)\coth(\sqrt{j\omega'})}{(1+\delta)^2\sqrt{j\omega'}} + \frac{2\delta}{(1+\delta)^2} + \alpha \quad (18)$$

The normalized impedance composes of real and imaginary components to show in the Nyquist plot.

Hence, $Z'(\omega') = Re(\omega') - jIm(\omega')$ (19)

, where

$$Re(\omega') = \frac{2\delta}{(1+\delta)^2\sqrt{\omega'/2}}\frac{\sinh(\sqrt{\omega'/2})\cos(\sqrt{\omega'/2}) - \cosh(\sqrt{\omega'/2})\sin(\sqrt{\omega'/2})}{\cosh^2(\sqrt{\omega'/2}) - \cos^2(\sqrt{\omega'/2})} + \frac{(1+\delta^2)}{(1+\delta)^2\sqrt{\omega'/2}}\frac{\sinh(\sqrt{\omega'/2})\cosh(\sqrt{\omega'/2}) - \sin(\sqrt{\omega'/2})\cos(\sqrt{\omega'/2})}{\cosh^2(\sqrt{\omega'/2}) - \cos^2(\sqrt{\omega'/2})} + \frac{2\delta}{(1+\delta)^2} + \alpha \quad (20)$$

$$Im(\omega') = \frac{2\delta}{(1+\delta)^2\sqrt{\omega'/2}}\frac{\sinh(\sqrt{\omega'/2})\cos(\sqrt{\omega'/2}) + \cosh(\sqrt{\omega'/2})\sin(\sqrt{\omega'/2})}{\cosh^2(\sqrt{\omega'/2}) - \cos^2(\sqrt{\omega'/2})} + \frac{(1+\delta^2)}{(1+\delta)^2\sqrt{\omega'/2}}\frac{\sinh(\sqrt{\omega'/2})\cosh(\sqrt{\omega'/2}) + \sin(\sqrt{\omega'/2})\cos(\sqrt{\omega'/2})}{\cosh^2(\sqrt{\omega'/2}) - \cos^2(\sqrt{\omega'/2})} \quad (21)$$

and the normalized angular frequency, $\omega' = \sqrt{\frac{\omega a C l^2(\sigma+\eta)}{2\sigma\eta}}$.

The calculated frequency dependence impedance, Z' can be used to obtain the capacitance of the device. The capacitance is the inverse of the product of frequency and the imaginary component of the frequency response [14].
It is expressed as $C = \frac{\sigma\eta}{Im(\omega')\omega(\sigma+\eta)l}$. (22)

The energy delivered by the device is corresponding to the area under the voltage-time plot. By integrating the normalized device voltage in Eq. (15), the normalized energy density is calculated as

$$E' = \left[1 - \frac{(1+3\delta+\delta^2)I'}{(1+\delta)^2} - \frac{\alpha I'}{2}\right]I'\tau + \frac{2I'^2}{(1+\delta)^2}\sum_{n=1}^{\infty}\frac{[(-1)^n+\delta]^2}{n^2\pi^2}(e^{-n^2\pi^2\tau} - 1) \quad (23)$$

III. Results and Discussion

The expression of capacitance and energy density in Eqs. (22) and (23) derived from the proposed supercapacitor model

are used to study the supercapacitor characteristics in frequency domain. This model is also applied to compute the capacitance obtained by previous results [5, 10] using similar device parameters for comparison.

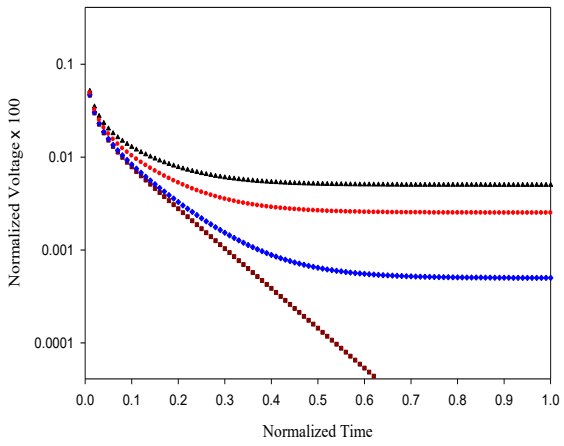

Fig. 2. The normalized voltage discharge for separator to electrode resistance ratio, α = 0 (square), 0.1 (diamond), 0.5 (circle) and 1 (triangle) at a normalized constant current, I' = 1 when electrode conductivity is high (solution to matrix conductivity ratio, δ = 0) in supercapacitor.

Figure 2 shows the discharge voltage for various separator to electrode resistance ratios at normalized constant current, I' = 1 in a supercapacitor. The voltage discharge very fast when no separator or low resistance for separator in the device for the case α = 0. It could be due to the high electrode resistance in the device which is normally avoided when selecting the electrode material. The type of electrode plays an important role in determining the performance of supercapacitor. The porosity of the electrode is low where few charges are capable to store in the device and causes the instability of the output voltage. The calculated result shows that there is a significant voltage drop of an order across the device when separator to electrode resistance ratio, α = 1 due to the potential drops across both the separator and electrode in this capacitor. The total resistance consists of the resistances from separator, solution and electrode in series.

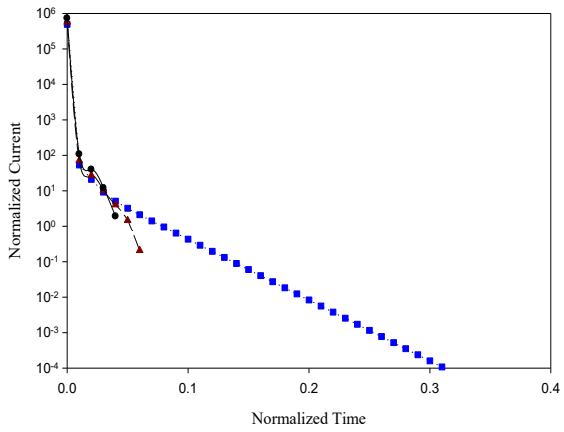

Fig. 3. The normalized current computed for solution to matrix conductivity ratio of δ = 0.1 (circle), 0.5 (triangle) and 1 (square) when α = 0 in supercapacitor.

Figure 3 shows the normalized current in a supercapacitor with no separator or low resistance for separator when α = 0. The current continues to flow as a good conductor when the electrical conductivity of the solution and electrode are equally important in the case solution to matrix conductivity ratio, δ = 1. The computed current shows that there is limited device current flow when the solution conductivity is low as δ decreases to 0.1. It explains that the low solution conductivity discourages the transportation of ion in the device. Moreover, it may be due to the blockage of ion transportation by the presence of low resistance separator. This is similar to the device studied by Newman *et al.* [5] using electric circuit model in the past research work.

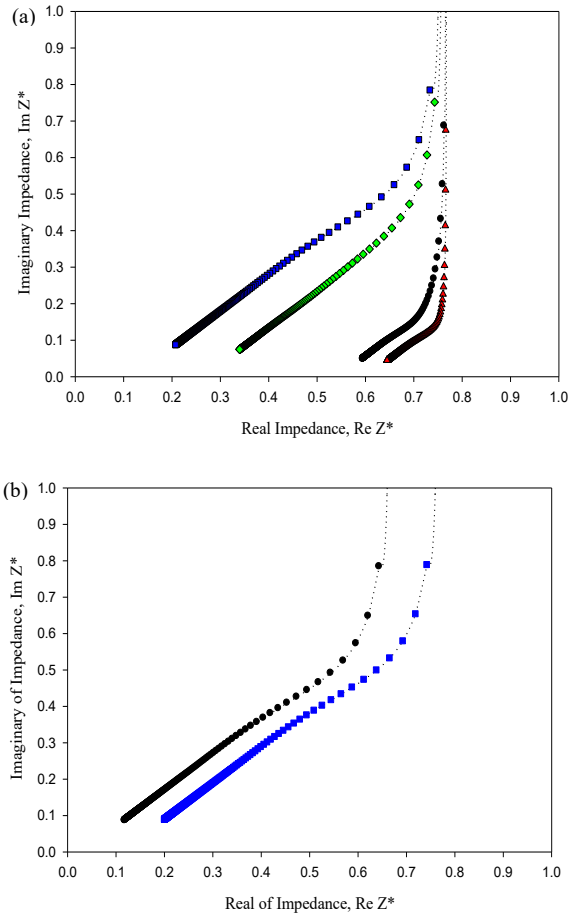

Fig. 4. (a) The normalized impedance plot for solution to matrix conductivity ratio of δ = 0.01 (square), 0.1 (diamond), 0.5 (circle) and 1 (triangle) when separator to electrode resistance ratio, α = 0.1. (b) The computed impedance characteristics using Newman *et al.*'s parameters (circle) with δ = 0.01 and α = 0.01 and Lin *et al.*'s parameters (square) with $\delta = 1\times10^{-6}$ and α = 0.11 in our model.

The device behaves conductive when solution to matrix conductivity ratio, δ of 0.01 in which the matrix conductivity is high in Fig. 4(a). The straight line in the plot explains the high electrical conductivity obeying Ohms' law for porous electrode in the device. The supercapacitor behaves toward metallic characteristics when solution to matrix conductivity ratio approaches unity at high real Z value shown in the plot. Indeed the presence of solution aids the ion transport in the device hence enhances the conductivity in particular at the interface between the solution and electrode. The device resistance contributes mainly from the solution and porous electrode when the separator resistance is low. By applying

the proposed supercapacitor model, Fig. 4(b) shows the impedance characteristic curves calculated using Newman *et al.*'s [5] parameters of $C = 30$ μF/cm^2 with $\delta = 0.01$ and $\alpha = 0.01$ and Lin *et al.*'s [10] parameters of $C = 20$ μF/cm^2 with $\delta = 1\times10^{-6}$ and $\alpha = 0.11$. Both results show the conductive behavior in these plots although there are some differences on material properties and device dimensional parameters. Their work focused on the low solution conductivity device.

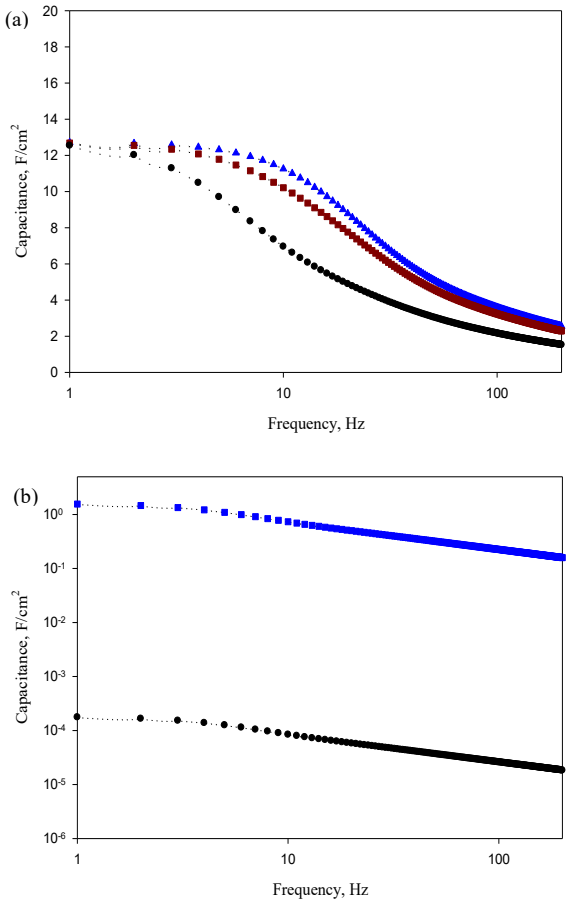

Fig. 5. (a) The computed capacitance for solution to matrix conductivity ratio, δ of 0.1 (circle), 0.5 (square) and 1 (triangle) with separator to electrode resistance ratio of $\alpha = 0.1$ in supercapacitor. (b) The computed capacitance for Newman *et al.* (circle) and Lin *et al.* (square) using the proposed supercapacitor model.

In Fig. 5(a), it is observed that the maximum capacitance of 12.71 F/cm^2 occurs at low frequency region in general device model. The capacitance decreases when the frequency increases to 200 Hz. The device capacitance increases toward ideal capacitor for the case of solution to matrix conductivity ratio, δ approaching unity. It is due to the uniformity of the current distribution when solution to matrix conductivity ratio is unity. It is observed that the capacitance value is getting smaller when the solution conductivity decreases in the device.

The supercapacitor model is applied to calculate the capacitance of 30 μF/cm^2 for double-layer supercapacitor from Newman *et al.* work as shown in Fig. 5(b). It shows that the proposed supercapacitor model fitted closely to Newman *et al.*'s result at 75 Hz using their device parameters in double-layer supercapacitor with the porous carbon electrodes. The dependence of δ is similar to our work but the numerical values are different for an order due to the differences of a few physical and device parameters used for thick device in their work. In this work, the maximum capacitance of 175.86 μF/cm^2 was calculated using their device parameters. In contrast, our model is not able to reproduce the assumed capacitance value of 20 μF/cm^2 from Lin *et al.* work in an electrochemical capacitor with hydrous ruthenium oxide ($RuO_2.xH_2O$) electrodes incorporating the double layer charges and surface faradaic processes. The maximum capacitance of 1.56 F/cm^2 was computed from our model. The difference of capacitance value of five orders with our result is due to the assumption of capacitance value in micron range made in their model. In our computational work, the capacitances computed in these results used the conductive behavior with inclusion of solution conductivity shown in Fig. 4(b).

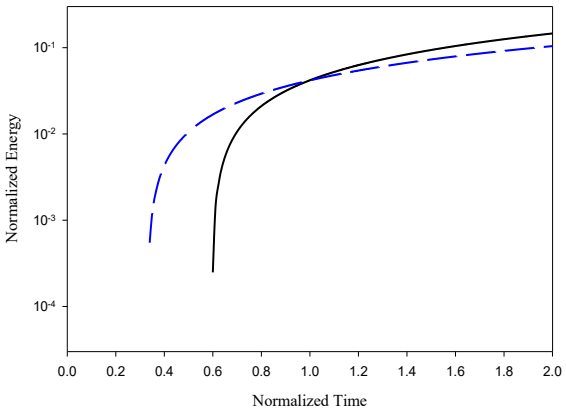

Fig. 6. The normalized energy for solution to matrix conductivity ratio, δ of 0.1 (solid-line) and 1 (dash-line) when separator to electrode resistance ratio is unity ($\alpha = 1$) in the supercapacitor.

Figure 6 shows more energy storage for solution to matrix conductivity ratio, δ of 0.1 when conductivity of porous electrode is high. Hence, the relatively low conductivity of the solution is capable to store energy with charge carriers accumulated on the electrodes in the device. In the case of the solution and electrode conductivities are equally high, it implies the high capacitance to achieve the high energy storage in the short period of time in this device. The current continues to flow uniformly in between the solution and electrode. It may function as a good supercapacitor to meet the requirements for renewable energy storage. On the other hand, it takes more time to accumulate the desired energy for separator to electrode resistance ratio of unity with the resistive separator inserted in the device. The additional separator resistance contributes to the overall device resistance.

IV. Conclusion

A supercapacitor model was developed to determine the capacitance of a supercapacitor using porous-electrode theory. The electrochemical impedance, capacitance and energy density of supercapacitor were calculated by applying the Laplace transform in proposed theoretical model. The maximum capacitance of 12.71 F/cm^2 was obtained at low frequency in this device. The proposed supercapacitor model will be used to simulate the electrical characteristics of polymer-based supercapacitor in near future.

ACKNOWLEDGEMENT

The authors gratefully acknowledge the Ministry of Higher Education Malaysia for the financial support under FRGS Grant (FRGS/1/2013).

REFERENCES

[1] L. Pilon, H. Wang and A. d'Entremont, "Recent Advances in Continuum Modeling of Interfacial and Transport Phenomena in Electric Double Layer Capacitors," *J. Electrochem. Soc.*, vol. 162, no. 5, pp. A5158-A5178, 2015.

[2] J. A. Stasera and J. W. Weidner, "Mathematical Modeling of Hybrid Asymmetric Electrochemical Capacitors," *J. Electrochem. Soc.*, vol. 161, no. 8, pp. E3267-E3275, 2014.

[3] F. A. Posey and T. Morozumib, "Theory of Potentiostatic and Galvanostatic Charging of the Double Layer in Porous Electrodes," *J. Electrochem. Soc.*, vol. 113, pp. 176-184, 1966.

[4] B. Pillay and J. Newman, "The Influence of Side Reactions on the Performance of Electrochemical Double-layer Capacitors," *J. Electrochem. Soc.*, vol. 143, pp. 1806-1814, 1966.

[5] A. M. Johnson and J. Newman, "Desalting by Means of Porous Carbon Electrodes," *J. Electrochem. Soc.*, vol. 118, pp. 510-517, 1971.

[6] T. Kadyka and M. Eikerling, "Charging Mechanism and Moving Reaction Fronts in a Supercapacitor with Pseudocapacitance," *J. Electrochem. Soc.*, vol. 161, no. 3, pp. A239-A246, 2014.

[7] H. Shi, "Activated Carbons and Double Layer Capacitance," *Electrochim. Acta*, vol. 41, pp. 1633-1639, 1996.

[8] C. J. Farahmandi, "A Mathematical Model of an Electrochemical Capacitor with Porous Electrodes," *Proc. Symp. Electrochemi. Capacitors*, vol. 96-25, pp. 167-179, 1997.

[9] V. Srinivasan and J. W. Weidner, "Mathematical Modeling of Electrochemical Capacitors," *J. Electrochem. Soc.*, vol. 146, no. 5, pp. 1650-1658, 1999.

[10] C. Lin, J. A. Ritter, B. N. Popov and R. E. White, "A Mathematical Model of an Electrochemical Capacitor with Double-layer and Faradaic Processes," *J. Electrochem. Soc.*, vol. 146, no. 9, pp. 3168-3175, 1999.

[11] C. Lin, B. N. Popov and H. J. Ploehn, "Modeling the Effect of Electrode Composition and Pore Structure on the Performance of Electrochemical Capacitors," *J. Electrochem. Soc.*, vol. 149, no. 2, pp. A167-A175, 2002.

[12] H. Kim and B. N. Popov, "A Mathematical Model of Oxide/Carbon Composite Electrode for Supercapacitors," *J. Electrochem. Soc.*, vol. 150, no. 9, pp. A1153-A1160, 2003.

[13] M. W. Verbrugge and P. Liu, "Microstructural Analysis and Mathematical Modeling of Electric Double-layer Supercapacitors," J. *Electrochem. Soc.*, vol. 152, no. 5, pp. D79-D87, 2005.

[14] A. J. Bard and L. R. Faulkner, *Electrochemical Methods: Fundamentals and Applications*, New York, USA: Wiley, 1980.